



Improved inland water levels from SAR altimetry using novel empirical and physical retracers



Heidi Villadsen^{a,*}, Xiaoli Deng^b, Ole B. Andersen^a, Lars Stenseng^a, Karina Nielsen^a, Per Knudsen^a

^aNational Space Institute, Technical University of Denmark, Elektrovej 327, 2800 Kgs. Lyngby, Denmark

^bSchool of Engineering, University of Newcastle, University Drive, Callaghan, NSW 2308, Australia

ARTICLE INFO

Article history:

Received 24 September 2015

Received in revised form 20 March 2016

Accepted 22 March 2016

Available online 29 March 2016

This manuscript was handled by Tim R. McVicar, Editor-in-Chief, with the assistance of Nikolaus Callow, Associate Editor

Keywords:

CryoSat-2
Satellite altimetry
Retracking
SAR
Inland water
SAMOSA

SUMMARY

Satellite altimetry has proven a valuable resource of information on river and lake levels where in situ data are sparse or non-existent. In this study several new methods for obtaining stable inland water levels from CryoSat-2 Synthetic Aperture Radar (SAR) altimetry are presented and evaluated. In addition, the possible benefits from combining physical and empirical retracers are investigated.

The retracking methods evaluated in this paper include the physical SAR Altimetry M₀de Studies and Applications (SAMOSA3) model, a traditional subwaveform threshold retracker, the proposed Multiple Waveform Persistent Peak (MWaPP) retracker, and a method combining the physical and empirical retrackers. Using a physical SAR waveform retracker over inland water has not been attempted before but shows great promise in this study.

The evaluation is performed for two medium-sized lakes (Lake Vänern in Sweden and Lake Okeechobee in Florida), and in the Amazon River in Brazil. Comparing with in situ data shows that using the SAMOSA3 retracker generally provides the lowest root-mean-squared-errors (RMSE), closely followed by the MWaPP retracker. For the empirical retrackers, the RMSE values obtained when comparing with in situ data in Lake Vänern and Lake Okeechobee are in the order of 2–5 cm for well-behaved waveforms. Combining the physical and empirical retrackers did not offer significantly improved mean track standard deviations or RMSEs. Based on these studies, it is suggested that future SAR derived water levels are obtained using the SAMOSA3 retracker whenever information about other physical properties apart from range is desired. Otherwise we suggest using the empirical MWaPP retracker described in this paper, which is both easy to implement, computationally efficient, and gives a height estimate for even the most contaminated waveforms.

© 2016 Elsevier B.V. All rights reserved.

1. Introduction

In recent years the availability of in situ lake and river levels has declined (Brakenridge et al., 2012), which is very unfortunate in a time with increasing focus on climate change and concern about freshwater resources. Satellite altimetry offers regular and global information about river and lake levels independent of infrastructure and governmental politics, which can greatly benefit the fields of hydrology, climate change detection, and flood/drought forecasting.

Satellite altimetry has been used for monitoring purposes of inland waters for more than 20 years, and is accepted as an important source of global inland water levels with a unique monitoring capability (Berry, 2006). The usefulness of satellite radar altimetry data both in near real-time and long-term applications has been

demonstrated in several studies, with purposes such as discharge modelling and flood warning (Neal et al., 2009; Biancamaria et al., 2011; Michailovsky et al., 2013). In addition to the scientific and practical advantages, satellite altimetry also provides a way of overcoming the difficulty of transboundary river management, which is often hindered by local governments considering their hydrological measurements as sensitive. Some studies have focused on lakes (Birkett, 1994; Cretaux and Birkett, 2006; Song et al., 2014; Schwatke et al., 2015a), while others have focused on rivers (Koblinsky et al., 1993; Birkett, 1998; Berry et al., 2005; da Silva et al., 2010; Jarihani et al., 2013; Maillard et al., 2015; Schwatke et al., 2015a), or wetlands (Zakharova et al., 2014). For a selection of relevant papers, the key results with regards to retracking method and obtained RMSE (root-mean-square-error) compared to in situ gauge data have been included in Table 1. Results over rivers vary much more (with averages in the decimetre range) due to several factors, such as a higher risk of

* Corresponding author.

Table 1

Overview of a selection of papers on inland water altimetry relevant to the current study (this paper has been added for completeness). Key results are identified by code: (1) Used retracers (2) RMSE from comparison with in situ gauges. For some of the earlier studies the used retracker was not stated in the manuscript, which is here marked as “Not listed”. Studies without comparison with in situ gauges at virtual stations (VS) have been left out.

Study	Mission(s)	Study area	Key results – 1: Retracker 2: Obtained RMSEs
Koblinsky et al. (1993)	Geosat (1986–1989)	Four locations on the Amazon River	1. Not listed 2. 20–120 cm
Birkett (1995)	TOPEX/Poseidon (T/P)	Lake Ontario (18,960 km ²), Lake Michigan (58,000 km ²), and Lake Superior (82,100 km ²)	1. T/P GDR data 2. 3–5 cm
Birkett (1998)	T/P	One location on the Paraguay River and several on the Amazon River	1. Not listed 2. Paraguay River: 10.7–13.5 cm. Amazon River: 19–75 cm
Birkinshaw et al. (2010)	Envisat and ERS-2	Mekong River (widths ≥ 0.4 km)	1. Not listed 2. Envisat: 44–65 cm ERS-2: 46–76 cm
da Silva et al. (2010)	Envisat and ERS-2	Five VS in The Negro River and Madeira River (widths of 0.2–1.7 km), 20 VS in the Amazon basin	1. Ice-1 and Ice-2 2. Negro/Madeira Rivers: ~ 34 cm (Envisat) and ~ 108 cm (ERS-2). Amazon River: ~ 48 cm (Envisat) and ~ 79 cm (ERS-2)
Jarihani et al. (2013)	Jason-2, Envisat, T/P, GFO, and Jason-1	Lake Eildon, Australia (138 km ²) and Lake Argyle, Australia (1000 km ²)	1. Ice-1/Ice-3 (Jason-2), Ice-1/Ice-2 (Envisat), Ocean retracker (T/P, GFO, Jason-1) 2. Lake Eildon: 28 cm/32 cm (Jason-2). Lake Argyle: 42 cm/138 cm (Envisat), 150 cm (T/P), 89 cm (GFO), 112 cm (Jason-1)
Michailovsky et al. (2012)	Envisat	20 VS in the Zambezi River, Africa	1. Not listed 2. ~ 58 cm (24–106 cm) when adjusting the obtained amplitude from altimetry
Yi et al. (2013)	Jason-1 and Envisat	Lake Baikal, Siberia (31,722 km ²)	1. Envisat: Ice-1 and a 50% Threshold Retracker (TR) Jason-1: Ice-1 and ocean (MLE4 type) 2. Envisat: 9.5 cm (Ice-1) and 12.1 cm (TR) Jason-1: 10.7 cm (ocean) and 9.7 cm (TR)
Schwatke et al. (2015a)	Envisat and SARAL	The Great Lakes: Lake Superior (82,100 km ²), Lake Huron (59,570 km ²), Lake Michigan (58,000 km ²), Lake Erie (25,744 km ²), Lake Ontario (18,960 km ²), 9 VS in the Amazon	1. Ice-1 and Brown retracker 2. Lakes: ~ 4.27 (2.92–5.34) cm for Envisat and ~ 3.83 (2.42–5.04) cm for SARAL. Amazon: ~ 32.3 (8.3–58.8) cm for Envisat, ~ 17.5 (7.8–31.8) cm for SARAL
Nielsen et al. (2015b)	CryoSat-2 SAR and Envisat	In situ and altimetry data compared for two lakes: Vänern (Sweden, 5650 km ²) and Lake Okeechobee (Florida, 1900 km ²)	1. Ice-1 (Envisat) and NPPR (CryoSat-2). CryoSat-2 SAR data were retracked using several empirical retrackerers. The NPPR method proved to be the most stable of them all 2. Lake Vänern: 5 cm (CryoSat-2) and 9 cm (Envisat). Lake Okeechobee: 8 cm (CryoSat-2) and 4 cm (Envisat)
Maillard et al. (2015)	Envisat and SARAL	São Francisco River, Brazil. Satellite altimetry and in situ gauges were compared for 16 locations	1. Ice-1 2. Envisat: ~ 66.8 (15.7–163.3) cm. SARAL: ~ 46.9 (2.2–134 cm)
Villadsen et al. (current study)	CryoSat-2	Lake Vänern (5650 km ²), Lake Okeechobee (1891 km ²), Amazon River near Óbidos (width of 2.2 km)	1. NPPR, MWaPP, and SAMOSA3 2. Lake Vänern: 10.9 (5.1) cm for NPPR, 5.0 (3.8) cm for MWaPP, and 3.5 cm for SAMOSA3. Lake Okeechobee: 61.8 (2.4) cm for NPPR, 12.6 (2.4) cm for MWaPP, and 2.1 cm for SAMOSA3. Amazon River: 33.3 (14.7) cm for NPPR, 38.5 (15.0) cm for MWaPP, and 15.3 cm for SAMOSA3

contamination from land signals caused by topography or the shape of the river, quality of in situ data, distance between virtual stations (VS) and river gauges, as well as a lower number of observations due to river widths. In Maillard et al. (2015) they found that the surrounding surface type was the most important factor for obtaining time series with low RMSEs over rivers, as the signals retrieved by the altimeter over dense vegetation were very different from the signals acquired directly over the water body.

With the launch of CryoSat-2 began a new era with its Synthetic Aperture Radar (SAR) altimeter. CryoSat-2 is the first altimetric mission to provide data with an along-track footprint size of just 300 m. With the reduced antenna footprint comes many advantages, especially for smaller water bodies, as the degree of contamination from land signals is significantly reduced in the along-track direction. Previous studies using CryoSat-2 data over inland water are scarce but include Tourian et al. (2015), where they used

several remote sensing methods to monitor the desiccation of Lake Urmia in Iran – here amongst Low Resolution Mode (LRM) data from the CryoSat-2 mission. In Nielsen et al. (2015b) lake levels were estimated for three small (8–40 km²) lakes in Denmark using CryoSat-2 SAR mode data, and they found an along-track precision of only 2–3 cm. Another study from Kleinhertenbrink et al. (2015) used SAR Interferometric (SARIn) data to monitor lake level changes on the Tibetan Plateau and Tian Shan. A challenge with CryoSat-2 is the geodetic orbit (ESA and Mullard Space Science Laboratory – University College London, 2012), which makes monitoring of inland water difficult. However, due to the 30-day sub-cycles, capturing seasonal signals in a time series is still possible if the water body is of a sufficient size. The ability to retrieve seasonal signals from CryoSat-2 data comparable to those from Envisat has previously been shown in the Ganges–Brahmaputra basin (Villadsen et al., 2015).

Several projects already provide historical inland water levels from altimetry through web databases, such as the European Space Agency (ESA) River&Lake project (<http://earth.esa.int/riverandlake>, Berry et al. (2005)), the Global Reservoir and Lake Monitor (http://www.pecad.fas.usda.gov/cropexplorer/global_reservoir/, Birkett et al. (2011)), the HYDROWEB database (<http://www.legos.obs-mip.fr/soa/hydrologie/hydroweb/>, Crétau et al. (2011)), and the Database for Hydrological Time Series of Inland Waters (DAHITI) database (<http://dahiti.dgfi.tum.de/en>, Schwatke et al. (2015b)). Of these four databases, DAHITI is the only one that provides heights from CryoSat-2 data. At DTU Space at the Technical University of Denmark a new data product has recently been developed that at the time of writing provides water level time series from CryoSat-2 for around 100 lakes around the world (<http://altwater.dtu.space>, Nielsen et al. (2015a)).

The quality of height estimates obtained from satellite altimetry can be improved with waveform retracking, where a correction is added to the initial range estimate obtained from the approximate two-way travel time of the pulse, which for CryoSat-2 is defined as the centre of the recorded range window. In this study the aim is to investigate the possibility of obtaining better heights by using several new retracking approaches, as retracking of inland water waveforms is still a maturing field. In total, there are three objectives of this manuscript: (1) To present the newly developed empirical Multiple Waveform Persistent Peak (MWaPP) retracker, which tries to remedy the erroneous heights obtained when specular surfaces in the measurement footprint contaminate the waveform – an effect known as snagging. The MWaPP retracker takes adjacent waveforms into account before choosing the location of the subwaveform to be retracked. (2) To test the abilities of the physical SAMOSA3 retracker over inland water. Up until now, SAR waveforms over inland water have been retracked using empirical retrackers only, apart from the study by Kleinharenbrink et al. (2014), where the cross-correlation between the observed waveforms and a simulated waveform was used to estimate the retracking correction. In this study it is shown that it is possible to retrack a large part of the waveforms with the SAMOSA3 (SAR Altimetry MOde Studies and Applications) retracker, which accommodates both ocean-like and specular waveforms. (3) In addition, this study investigates the possible benefits of combining empirical and physical retrackers.

2. Data

2.1. CryoSat-2 20 Hz SAR waveforms

CryoSat-2 was launched by ESA on the 8th of April 2010 to monitor variations in the cryosphere, i.e. the marine ice cover and continental ice sheets. The primary payload on-board CryoSat-2 is the Synthetic Aperture Interferometric Radar Altimeter (SIRAL), which is a state-of-the-art altimeter working in three different measurement modes depending on a geographical mode mask (Wingham et al., 2006). As this study has been part of the European Union's 7th Framework Programme project Land and

Table 2
Magnitudes of the different geophysical corrections applied for inland water altimetry as listed in The CryoSat Product Handbook (ESA and Mullard Space Science Laboratory – University College London, 2012).

Correction	Range of correction
Dry troposphere	1.7–2.5 m
Wet troposphere	0–50 cm
Ionosphere	6–12 cm
Ocean loading tide	–2 to +2 cm
Solid Earth tide	–30 to +30 cm
Geocentric polar tide	–2 to +2 cm

Ocean Take Up from Sentinel-3 (LOTUS), the focus of the work presented in this paper has been on SAR mode, which is also the mode that the Sentinel-3 Ku/C Radar Altimeter (SRAL) altimeter on the upcoming Sentinel-3 mission will operate in. ESA provides CryoSat-2 data in Level 1 (L1) and Level 2 (L2) modes. L1 contains the orbit information and the echoes received by the altimeter, also called waveforms. L2 contains the geophysical corrections (see list of applied corrections in Table 2) as well as a height estimate. The basis for our data processing is the 20 Hz L1b datasets, which we retracked using three different retrackers (explained in Section 3), and the L2 datasets provided by ESA.

The general mission specifications of CryoSat-2 are shown in Table 3. The reduced footprint area for SAR is significantly smaller compared to conventional LRM altimetry. The long repeat period of 369 days should also be noted as it makes monitoring inland water slightly more difficult compared to traditional missions such as Envisat, which has a repeat period of 35 days. The orbit configuration of CryoSat-2 results in a much higher ground track density, but brings with it a decreased temporal resolution. More information about the CryoSat-2 mission can be found in ESA and Mullard Space Science Laboratory – University College London (2012), and a longer explanation of SAR altimetry is found in Raney (1998), where SAR altimetry was first proposed and described as Delay/Doppler altimetry.

2.2. Water mask: Global Lakes and Wetlands Database (GLWD)

Waveforms retrieved over the study areas presented in Section 2.3 are extracted using the water masks GLWD-1 and GLWD-2, which are products from the Global Lakes and Wetlands Database (Lehner and Doll, 2004). The masks were derived from a variety of existing maps, data and information by the World Wildlife Fund (WWF) and the Center for Environmental Systems Research, University of Kassel, Germany. The product is available on global scale (1:1 to 1:3 million resolution), and can be downloaded as a shapefile from the WWF website (<https://www.worldwildlife.org/pages/global-lakes-and-wetlands-database>). The Level 1 product consists of the 3067 largest lakes and the 654 largest reservoirs worldwide. Level 2 comprises permanent water bodies with surfaces areas down to 0.1 km², excluding the water bodies contained in GLWD-1.

2.3. Study areas

This section briefly describes the chosen study areas and the availability of in situ data. The choice of study regions was limited by the availability of SAR data from CryoSat-2 (CryoSat-2 only operates in SAR mode over certain areas), the existence of in situ data, and the presence of acquired ocean-like waveforms. The SAMOSA3 model assumes a completely homogeneous surface within the measurement footprint, which is not always necessary in order to obtain an ocean type waveform, but the shape of the

Table 3
Satellite and altimeter specifications for the CryoSat-2 mission (ESA and Mullard Space Science Laboratory – University College London, 2012).

Mission specifications	CryoSat-2 SAR (SIRAL)
Mission length	April 2010 –
Frequency	13.575 GHz (Ku)
Bandwidth	320 MHz
Footprint size along-track	300 m
Footprint size across-track	7.7 km
Footprint area	4.9 km ² for SAR
Altitude	717 km
Inclination	92°
Latitudinal limit	88°
Repeat period	369 days (30 day sub-cycle)

acquired waveforms might be affected by the degree of heterogeneity of the underlying surface. In addition, when extracting time series from CryoSat-2 over rivers and lakes, the chosen water body has to have a certain length in the East–West direction in order to make it possible to utilize the orbit sub-cycles and thereby obtain a seasonal signal by using water levels from several tracks.

2.3.1. Lake Vänern

Lake Vänern is the largest lake in Sweden and in the European Union with an area of 5650 km² (Seppl, 2005) and is divided into two basins as seen in Fig. 5(a). The eastern basin is the larger, deeper one, and contains most of the inlets (Dave et al., 2015). The average depth of the lake is 27 m with a maximum depth of 106 m. Although there are some topographic variations around the lake, the highest point that is within reach of satellite footprint is Kinnekulle (270 m above sea level) on the south-eastern border. The northern drainage basin is dominated by forest, whereas the southern regions mostly consist of agriculture. The shoreline is generally irregular and complex. Sandy beaches and dunes, rocks, flat-rock pine forest, and bilberry spruce forest cover the islands and skerries in the archipelago. With winter temperatures below 0 °C, Lake Vänern might be ice-covered in certain areas, and during long and cold winters, the entire lake surface will freeze over, however, this is not taken into account in this study and heights are retrieved and compared to in situ data for all seasons.

Daily gauge data for Lake Vänern are available from the Swedish Meteorological and Hydrological Institute (SMHI, <http://www.smhi.se/klimatdata/hydrologi/>) and are referenced to the Swedish height system Riket höjdsystem 1900 (RH 00).

2.3.2. Lake Okeechobee

Lake Okeechobee (see Fig. 5(b)) is the largest freshwater lake in Florida with an area of 1900 km². For its size it is very shallow with an average depth of only 2.7 m (Beaver et al., 2013). Lake Okeechobee is a part of the Kissimmee–Okeechobee–Everglades ecosystem (Dyer and Garza, 2004), and is mainly surrounded by wetlands. Due to the shallow depths compared to surface area, Lake Okeechobee is very sensitive to tropical storms and precipitation in general.

In situ data from Okeechobee were obtained from the National Water Information System (<http://waterdata.usgs.gov/nwis>), and are relative to National Geodetic Vertical Datum of 1929 (NGVD 29). The daily water levels are means of 14 gauges placed in and around the rim of the lake.

2.4. Amazon River near Óbidos

The Amazon River is the largest river in the world with respect to discharge and has a dry season width of several kilometres – sometimes as much as 48 km in the wet season. The properties and width of the Amazon River provides a good testing ground for the method developed in this study, since most types of waveforms will be present here. The stretch chosen for this study surrounds a gauge station in Óbidos, Brazil, as seen in Fig. 5(c). In this region, the northern bank of the Amazon River is constrained by higher grounds, whereas the southern banks are much lower and often flooded (Rudorff et al., 2014). Daily water levels were obtained through the The Observation Service SO HYBAM website (<http://www.ore-hybam.org>, Cochonneau et al. (2006)).

3. Methods

This section briefly describes the basic theory of satellite altimetry, the waveform retracking methods used, the steps of the algorithm developed in this study for combining physical and

empirical retrackers, and the general data handling, such as the initial classification of waveforms and the minimization of the bias that is observed when combining retrackers.

It all begins with the satellite radar altimeter emitting a microwave pulse towards the surface of the Earth. At the surface the pulse is reflected back into space where it is received by the altimeter. The returned power echo is called a waveform and the shape of the retrieved waveform is related to the complexity of the entire illuminated surface within the measurement footprint. In general, waveforms retrieved over small, calm inland waters will have a single strong peak due to concentrated power returns, and those obtained over large, rough waters will have ocean-like shapes with a steep leading edge and a slowly decaying trailing edge. Lastly, waveforms retrieved over inhomogeneous terrain will have a very complicated shape with multiple peaks.

Based on the retrieved echo the time of the arrival of the reflection from the ground can be determined; this is done by measuring the two-way travel time of the microwave pulse. The height of the surface (H) above the geoid can be determined as given in Eq. (1).

$$H = H_{alt} - H_{range} - N_{geoid} \quad (1)$$

The surface height, H , depends on the altitude of the satellite above the reference ellipsoid, (H_{alt}), and the range (H_{range}), which is the distance between the satellite and the sensed surface below. N_{geoid} is the geoid height above the reference ellipsoid, which is subtracted in order to reference the water level to the geoid, since this is a more appropriate reference for inland water bodies. All retracked heights presented in this study were transferred from the WGS84 ellipsoid to the EGM08 geoid (Pavlis et al., 2012).

H_{range} is found by retracking the waveform received by the altimeter, i.e. finding the point in time when the signal from the surface directly beneath the satellite (also called nadir) was received. The range to the retracked bin in the waveform is calculated as follows,

$$H_{range} = \frac{c}{2}WD + H_{retrack} + H_{geo}, \quad (2)$$

where c is the speed of light, WD is the window delay in seconds relative to the central range bin (see Fig. 1), $H_{retrack}$ is the retracking correction, which depends on the chosen retracking routine, and H_{geo} is the sum of the applied geophysical corrections. The waveform received by the altimeter consists of a number of bins, each containing a power value corresponding to a certain distance from the satellite. An example of a SAR waveform is shown in Fig. 1. The CryoSat-2 SAR waveforms consist of 128 bins with a bin width of 23.42 cm, which corresponds to a range window of ~30 m.

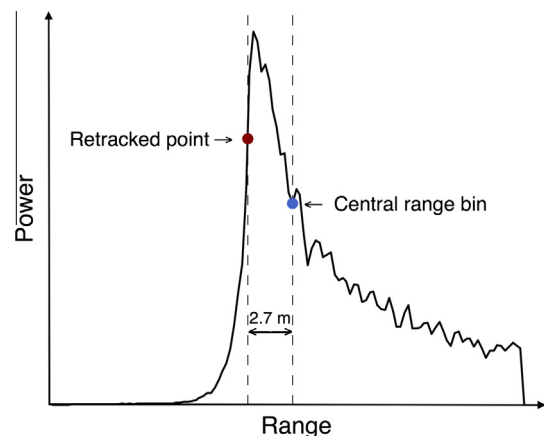


Fig. 1. Example of SAR mode CryoSat-2 waveform showing the central range bin and the retracking point.

Precise estimation of the retracking correction is especially important over topographic surfaces, where the on-board tracking system struggles with maintaining the reflection from nadir in the central range bin, since this is predicted from the position of the previous waveforms (Gommenginger et al., 2011). As seen in Fig. 1, the heights estimate is very sensitive to retracking. More details on the retrackers chosen for this study can be found in the following subsections.

3.1. Snagging

One of the biggest issues with satellite altimetry over non-homogenous surfaces such as land and inland water is off-ranging, also called hooking or snagging (Fetterer et al., 2013; Armitage and Davidson, 2014). Snagging and hooking occurs when the on-board tracking system is dominated by specular surfaces that are located off-nadir, which leads to incorrect height estimates. Specular surfaces are most often shallow or calm water bodies, which reflects the signal from the altimeter without the scattering caused by rougher surfaces. The presence of these calm waters is often seen near the shore of lakes, or in areas prone to flooding.

Hooking occurs in the along-track direction when a bright target in front of the nadir location leads to a parabolic profile in the waveforms as the satellite flies over the specular surface. The parabolic shape appears because the radar pulse propagates with a circular wavefront, and the target enters and leaves the measurement footprint (Gomez-Enri et al., 2010; Quartly, 2010). The hyperbolas caused by the hooking effect are only visible in LRM, where the large, circular footprint allows for off-ranging in both the along- and across-track directions. The hooking effect can easily be corrected for by fitting curves to the along-track hyperbolas, even over rivers (da Silva et al., 2010; Maillard et al., 2015; Schwatke et al., 2015a).

For SAR altimetry hooking issues are negligible due to the smaller footprint, which is achieved by the Doppler processing and has an along-track size of just ~ 300 m. Only across-track off-ranging, called snagging, will cause these range errors. Unfortunately, there are no hyperbolic curves to be identified, fitted, and subsequently removed. The positive effect of the higher across-track resolution on snagging occurrences in SAR altimetry was also shown in Thibaut et al. (2014), where they investigated coastal waveforms. In general, the SAR altimeter waveforms will be much more affected by land signals if the track lies parallel to the coastline compared to a perpendicular target angle due to the dimensions of the measurement footprint.

3.2. Empirical retrackers

The two empirical retrackers presented here use a simple threshold approach on a subwaveform to estimate the epoch. The two methods differ in the way that the subwaveform is extracted; the Narrow Primary Peak Retracker (NPPR) focuses only on the current waveform, whereas the Multiple Waveform Persistent Peak (MWaPP) retracker developed for this study takes adjacent waveforms into account.

3.2.1. The Narrow Primary Peak Retracker (NPPR)

When using the NPPR method the subwaveform is extracted by identifying the bins where the primary peak begins and ends. This is done by looking at the evolution of the power in the reflected waveform as described in Jain et al. (2015), Vignudelli et al. (2010) and Bao et al. (2009). Once the subwaveform has been extracted the retracking point is determined as the point where the subwaveform exceeds a chosen threshold. Finally, the algorithm finds the decimal range bin where the waveform exceeds

the threshold using linear interpolation between the two adjacent bins. The chosen threshold should depend on the underlying surface, with lower thresholds ($\sim 50\%$ for SAR) for ocean and ice sheets, and higher thresholds for ice leads and inland water. For this study a threshold of 80% to determine the retracking point is used, which has previously been done in Nielsen et al. (2015b) and Villadsen et al. (2015).

3.2.2. The Multiple Waveform Persistent Peak (MWaPP) retracker

For this study the new MWaPP retracker was developed, which looks at adjacent waveforms in order to determine the best sub-waveform for retracking. In this way it is possible to identify persistent peaks, which are expected to represent the underlying water body of interest. Looking at neighbouring waveforms can help alleviate snagging issues, where a waveform is dominated by reflections from points off-nadir. The method presented here does not average waveforms, but simply tries to determine the bins in the waveform where the reflection from the water surface at nadir is most likely found. Since the range to the water body at nadir should be the same in all waveforms, off-nadir echoes will not dominate the averaged waveform. The proposed retracking method consists of several steps, which are illustrated in Fig. 2.

For each waveform acquired above the water body, the heights corresponding to all bins are determined according to Eq. (1). This yields $N_w \times N$ height estimates, where N_w is the number of waveforms in the track and N is the number of bins in each waveform. Thus, a height is estimated for each $k = 1:128$ and $p = 1:N_w$ for CryoSat-2 SAR mode waveforms.

$$H^{all}(p, k) = H_{alt}(p) - \frac{c}{2} WD + w_b(k_0 - k) - H_{geo}(p) - N_{geoid}(p), \quad (3)$$

where H_{alt} is the satellite altitude, c is the speed of light, WD is the window delay, w_b is the bin width (0.2342 m for CryoSat-2 SAR mode waveforms), k_0 is the nominal range bin number (64 for CryoSat-2 SAR), H_{geo} is the sum of the applied geophysical corrections, and N_{geoid} is the geoid correction.

The surface height span of all waveforms within each track is determined as $\min(H^{all}):\max(H^{all})$ and the waveforms are oversampled to 1 cm height intervals using linear interpolation to derive the interpolated waveforms W_p^{int} . This allows for aligning the waveforms with respect to the obtained surface height instead of bin number.

For each W_p^{int} , the average of the current and the four nearest waveforms is calculated. Since the height of the water body at nadir should be the same for all observations, an average of waveforms is not dominated by off-nadir echoes and can be used to determine the subwaveform, which holds the nadir reflection. The five waveforms will be different from each other due to off-nadir contamination caused by varying surface cover or topography.

$$W_p^{ave} = \sum_{\max(p-2,1)}^{\min(p+2, N_w)} W_p^{int} \quad (4)$$

For each of these averaged waveforms, W_p^{ave} , the first peak that exceeds 20% of the maximum power is flagged. This is assumed to represent the water level common to all five waveforms. In the original L1B waveforms, the peak closest to the flagged peak from the averaged waveform is found, and a subwaveform consisting of the three previous and following bins around this peak is extracted. The off-centre-of-gravity (OCOG) amplitude (Vignudelli et al., 2010), A , is then calculated for the extracted subwaveform, which consists of N bins of which all but 7 are zero. The point where the subwaveform exceeds 80% of A is marked as the retracking point.

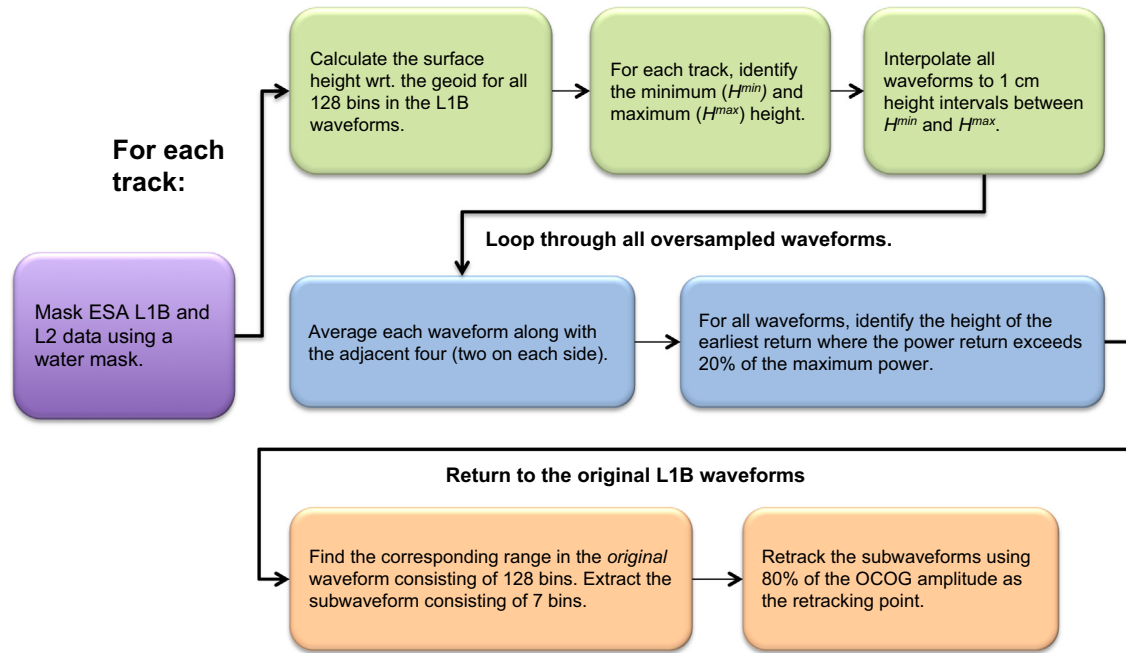


Fig. 2. Flowchart describing the MWaPP method.

$$A = \sqrt{\frac{\sum_{i=5}^{N-5} P_i^A(t)}{\sum_{i=5}^{N-5} P_i^2(t)}} \quad (5)$$

To illustrate the benefits of the MWaPP retracker, some intermediate results for an ascending track crossing Lake Okeechobee in Florida on December 29th, 2010, are shown in Fig. 3. The map in Fig. 3(a) shows the location of a specific waveform and highlights the adjacent waveforms. As seen from the retracked heights in Fig. 3(b) the standard NPPR retracker fails to determine the leading edge of the nadir reflection and instead retracks the echo coming from an off-nadir bright target located near the coast. As seen, the MWaPP retracker is able to determine a much more stable water level. Fig. 3(c) shows how the leading edges of the lake surface reflection are not aligned when the waveforms are referenced to bin number. However, when oversampling the waveforms and referencing them to surface height, a persistent leading edge appears around a height of 4–5 m and it becomes possible to extract the correct subwaveform.

3.3. The physical SAMOSA3 retracker

SAR altimeter waveforms are different from waveforms from conventional altimetry in the way that the power waveform is much more focused with a steeper leading edge and a faster decaying trailing edge. The SAMOSA (SAR Altimetry MODE Studies and Applications) project has developed new theoretical models necessary to retrack SAR mode waveforms in order to build on the theoretical knowledge and practical experience needed for the CryoSat-2 and Sentinel-3 missions (Jain, 2015; Dinardo et al., 2013). Information on the details of the development of the SAMOSA processing model can be found in Ray et al. (2015), Dinardo et al. (2013). The current model, which is used for this study, is the third version and therefore called SAMOSA3.

The SAMOSA3 model used for this study exists in two modes (Jain et al., 2014); the standard mode for ocean waveforms (hereafter called SAMOSA3-O), and a mode adapted for lead type waveforms where the trailing edge is a lot steeper due to a more specular surface reflection (hereafter called SAMOSA3-L). Since

inland water, like leads, can cause very specular waveforms, SAMOSA3-L is included in this study. The retracking correction is estimated in both modes. In ocean mode the significant wave height can be estimated and for the lead mode the roughness can be estimated. For this study only the ability of the SAMOSA3 retracker to fit the epoch (retracking point) is interesting, but it is worth noting the ability of the retracker to fit other parameters as well, as these might be useful for other studies.

In this study, it was found that the SAMOSA3 retracker only provide more precise height estimates if the correlation between the fitted waveform and the observed waveform was higher than 0.99 in the ten bins closest to the estimated epoch. In many cases ($\approx 40\%$) the SAMOSA3-L model fits the same waveforms that can be fitted with the SAMOSA3-O model, and sometimes the SAMOSA3-L fit will even be better. Waveforms that were classified as ocean-like were therefore fitted with both the SAMOSA3-O and the SAMOSA3-L model. If both the SAMOSA3-O and the SAMOSA3-L models provided fits with correlations higher than 99%, the retracking correction belonging to the model with the lowest sum of errors in the 10 closest bins of the epoch was chosen. This approach was chosen since the correlation did not always reveal the best fit.

Some examples of the ability of the two SAMOSA3 models to fit the CryoSat-2 waveforms are shown in Fig. 4. The results from an ocean-like waveform are shown in the graph to the left and the corresponding results are shown for a specular waveform to the right. Both SAMOSA3 models fit the ocean-like waveform, with correlations of 99.6% and 99.8% for the SAMOSA3-O and the SAMOSA3-L, respectively. The two fits for the specular example in Fig. 4 had correlations of 72.7% and 99.6% for SAMOSA3-O and SAMOSA3-L, respectively.

3.4. Data handling

The data handling consisted of several steps, as multiple retracker will be used for the retracking procedure where the physical and empirical retracker are combined, which requires some extra precautions.

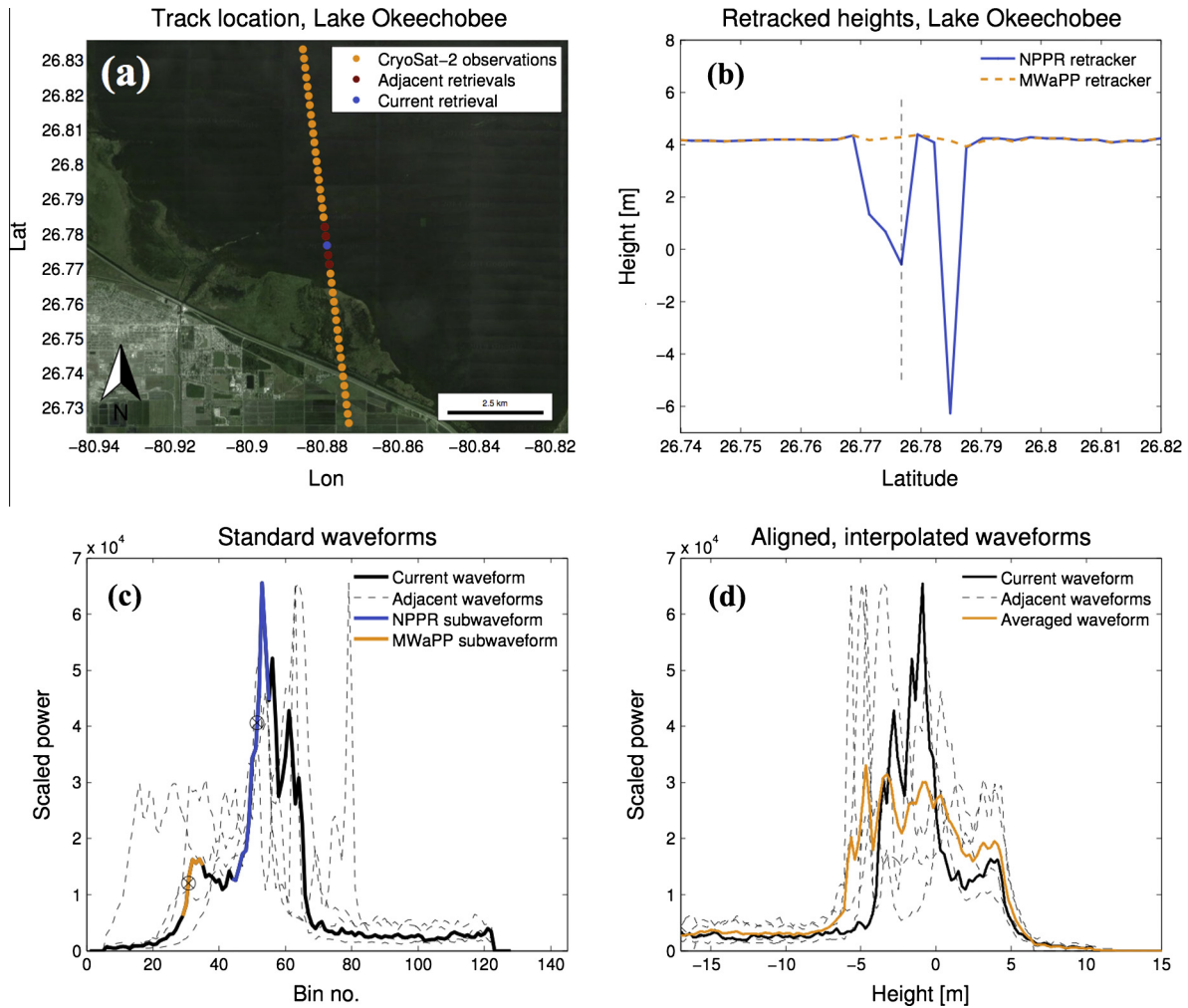


Fig. 3. An ascending track over Lake Okeechobee in Florida, December 29th, 2010. (a) Part of the track with the current observation (blue) and its adjacent points (red) highlighted, (b) the retracked heights obtained from both the NPPR retracker (blue) and the proposed MWaPP retracker (yellow), (c) the current (solid) and the four adjacent (dashed) waveforms along with the subwaveforms and retracking points obtained with the NPPR retracker (blue) and the proposed MWaPP retracker (yellow), and (d) the aligned and oversampled current (solid), adjacent (dashed), and averaged waveforms (yellow). (For interpretation of the references to colour in this figure legend, the reader is referred to the web version of this article.)

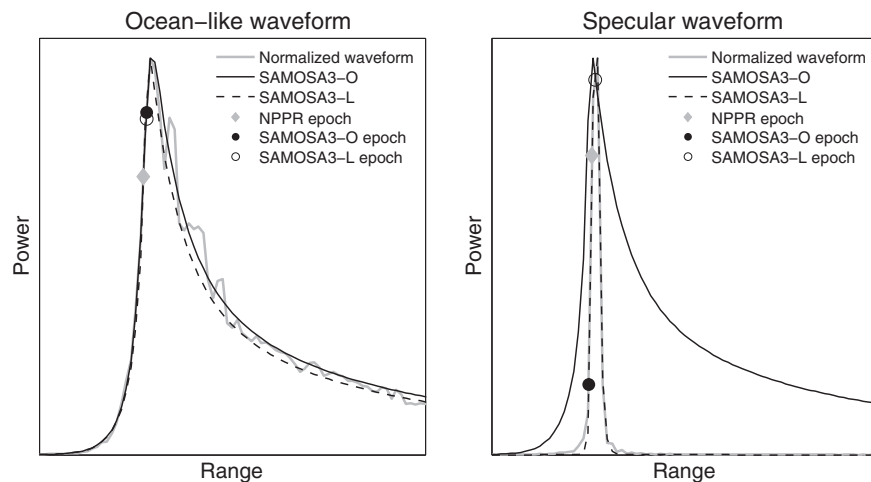


Fig. 4. The fits of SAMOSA3-O and SAMOSA3-L for an ocean-like (left) and a specular (right) waveform retrieved over Lake Okeechobee, Florida. The estimated epochs for each retracking method are also shown for comparison on the retrieved waveform.

1. The data are masked with the GLWD described in Section 2.2.
2. Waveforms that seem appropriate to retrack using the physical retracker are isolated by waveform classification. The waveforms are divided into 12 classes based on the shape of the power echoes using a Naive Bayes classifier. The Naive Bayes classifier was set up using a training set of approximately 6000 waveforms over inland water. This training set consist of most waveform types and was used for all three study regions.
3. All waveforms are retracked using the NPPR retracker and the proposed MWaPP retracker. Suitable waveforms are retracked using the SAMOSA3 retracker depending on the classification results, and heights for which the correlation between the observed and the modelled waveform is higher than 99% are accepted.
4. The worst outliers are removed by discarding all observations more than two standard deviations from the track mean – the outlier detection was performed twice as this was found to be most effective without removing too many observations. Tracks with fewer than six observations left were excluded from the study.
5. For the retracking procedure where the physical and empirical retracker are combined, an offset is introduced due to the different retracking routines. To reduce this offset and obtain a seamless transition when switching between retracker, the bias between them are minimized using a neural network approach as done in Idris (2014). The neural network is able to identify and model highly complex relationships between functions. Firstly, the neural network is trained by supplying it with input and output datasets. In this study the input data are the retracked heights obtained with the SAMOSA3 retracker, and the output values are the results from the empirical retracker (either the NPPR or the MWaPP retracker). The neural network then tries to minimize the difference between these two datasets. For each study region, the training set consists of 30% of the entire dataset. This method does not modify any retracking parameters, but simply adjusts the heights from the physical SAMOSA-3 model according to the model obtained through the neural network. More detailed information on the use of neural networks can be found in Beale et al. (2015). In the end, there will be five water level datasets:
 - (a) NPPR: Heights obtained using only the NPPR retracker.
 - (b) MWaPP: Heights obtained using only the proposed empirical retracker.
 - (c) Combined (NPPR): Heights obtained using a combination of the SAMOSA3 and the NPPR retracker. The bias was minimized using the NPPR heights for the training set.
 - (d) Combined (MWaPP): Heights obtained using a combination of the SAMOSA3 and the proposed MWaPP retracker. The bias was minimized using the MWaPP heights for the training set.
 - (e) SAMOSA3-O: Heights obtained using *only* the results from the traditional SAMOSA3 model for ocean-like waveforms.
6. For each track a mean is calculated, which is to be used for time series.

Due to the slope of the Amazon River, the track means used to derive the time series were detrended in the zonal direction similar to Villadsen et al. (2015) using the retracked heights derived in this study. The slope of the Amazon was estimated to be around 1 m per degree longitude by fitting a linear polynomial to the height estimates as a function of longitude.

For Lake Vänern and Lake Okeechobee the track means obtained from the various retracking methods were compared with in situ data. The offsets between the retracked data and the in situ data were removed prior to creating the time series by adjusting the level of the retracked datasets so the time series had the same

mean values as the in situ data. As such, the accuracy of the altimetric heights will not be discussed. Instead, the evaluation comprised of a comparison of range precisions and RMSEs.

When range precision is mentioned in this study we are referring to the precision of the mean (as in Nielsen et al. (2015b)), i.e. the mean standard deviation of each track crossing the study area in question.

4. Results

4.1. Waveform classification

The spatial distributions of the retracker used for Lake Vänern, Lake Okeechobee, and the Amazon River are shown in Fig. 5. The results reveal that all three types of retracker (SAMOSA3-O, SAMOSA3-L, and empirical) are seen in each study area. The degrees to which they are used, however, depend on the characteristics of the water body.

In Lake Vänern, which is the largest lake in this study, the SAMOSA3-O retracker is the most commonly used retracker in the central parts of the lake and is used for 32.9% of all waveforms retrieved over the lake. For some of the ocean-like waveforms the SAMOSA3-L retracker provides a better fit, and especially in the south borders of the western part of the lake the SAMOSA3-L retracker is used to fit more specular waveforms near the shore. In 51% of the cases the empirical retracker is chosen, especially in the vicinity of the shore where the waveforms get more complex due to contamination from land signals. For Lake Okeechobee the same pattern is seen with slightly more waveforms retracked with the lead adaptation of the SAMOSA3 retracker.

The distribution of assigned classes is slightly different in the Amazon River (see Fig. 5(c) with a larger number of empirically retracked waveforms. This agrees well with our expectations, as the Amazon River is smaller in size and has a channel pattern that is more complex compared to the regular shapes of the lakes. All of these characteristics are bound to produce more waveforms that are either noisy or specular, which the SAMOSA3-O model will not be able to fit. It is also seen that the specular waveforms are found in the narrow parts of the Amazon and its tributaries, whereas the SAMOSA3-O model is mostly used for waveforms retrieved over the wider stretches.

4.2. Comparison of retracking methods

To compare the different retracking methods some examples of the results for a couple of tracks crossing Lake Vänern and the Amazon River are shown in Figs. 6 and 7, respectively. Looking at the detailed plot in Fig. 6(c) it is clearly seen that the results from the MWaPP retracker are less noisy, such as the heights retrieved around 58.86°N. There are of course exceptions to this, and the sudden decrease in surface height around 58.58°N looks unnatural and must be a retracking error. However, in general the MWaPP approach appears to provide the best results.

The example over the Amazon River in Fig. 7 shows that the two pure empirical retracker give similar results for most waveforms. It was observed that the results from the combined method varies a lot regardless of the size of the training set used for the neural network.

4.3. Standard deviations of overpasses

The mean standard deviations, for all tracks for each study area are given in Tables 4 and 5 for all observations and observations where both SAMOSA3-O and SAMOSA3-L could have been used, respectively. The latter comparison was done to see how well the

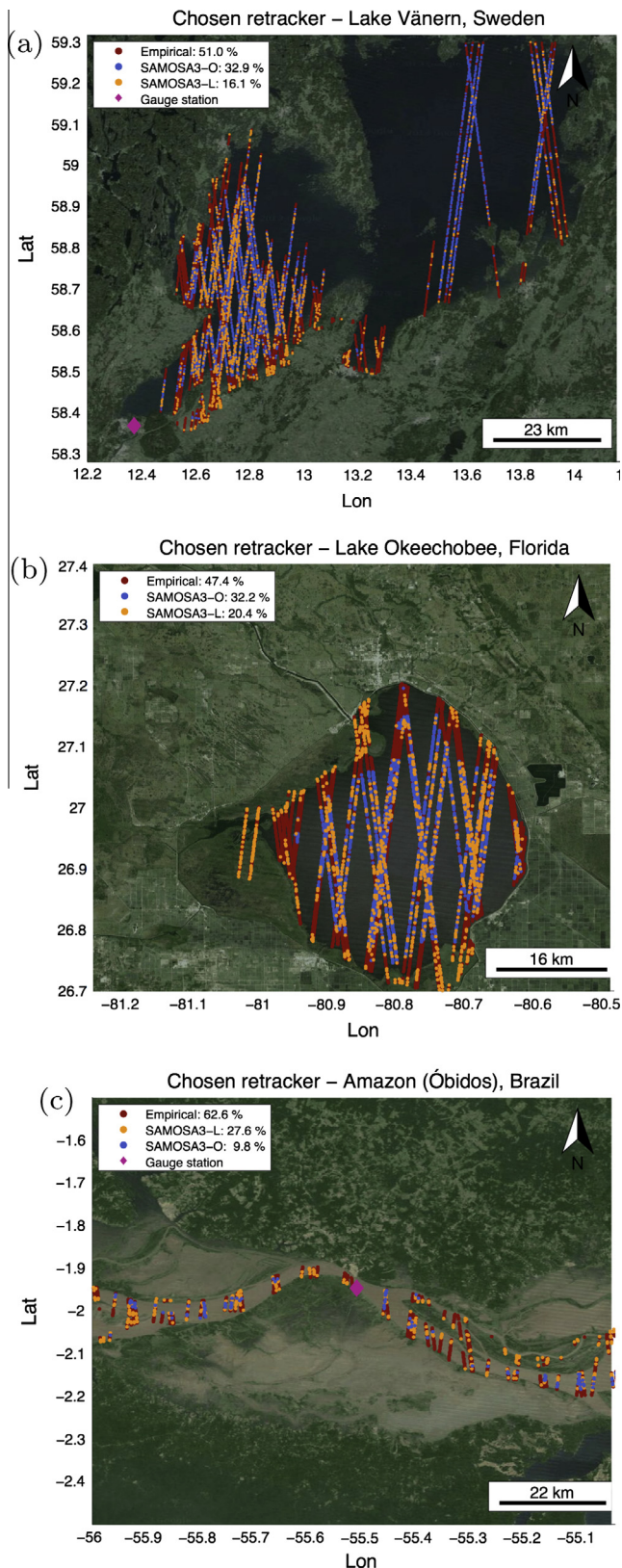


Fig. 5. Classification results over the three different study areas. Distributions as well as percentages showing where and how frequently the different retrackers were used.

SAMOS3-O retracker performs compared to the empirical retrackers. The standard deviations are a measure of the range precision and is mostly affected by the location of the track with

respect to the shore of the lake/river and the number of observations within each track. Higher standard deviations are usually seen for overpasses close the coastline or in data acquired over heterogeneous surfaces, where a high number of waveforms within the track might be contaminated.

From Table 4 it is seen that the MWaPP retracker has the lowest standard deviation of 9.1 cm over Lake Vänern, which is to be expected since this method will alleviate some snagging cases that a simple outlier removal method will not detect. The combined method where the MWaPP retracker has been used also performs well with a mean standard deviation of 9.8 cm. The performance of the NPPR retracker is not as good with standard deviations around 15–16 cm for both the purely empirical and the combined datasets. For comparison the results from the ESA L2 product have been included. As seen from the results, the L2 product from ESA does not provide stable heights over inland water and other retrackers should be used. In general the standard deviations are expected to decrease with increasing size of the water body (due to the higher chance of the underlying surface being homogeneous), which is what we see for the MWaPP methods.

Table 5 shows the track standard deviations only including retracked heights obtained from waveforms that could be fitted with both SAMOSA3 retrackers, which leaves us with only the well-behaved waveforms. Looking at only these waveforms allows for a fair comparison of the various retrackers, and as expected the range precision increases in general for all retracking methods. Comparing precisions between study areas becomes somewhat misleading, as the number of remaining observations for the smaller water bodies is very low (e.g. 2 SAMOSA3 fits per Amazon track). One should therefore only compare values for the same study area.

For Lake Vänern we see that the highest precisions are obtained when using just the SAMOSA3-O retracker, which is what we would expect considering the size of the lake.

For Lake Okeechobee and the Amazon River we also get the lowest standard deviations when using only the SAMOSA3-O retracker. It should be noted that for all methods apart from the ESA L2 product, the precision only varies within one centimetre (1.1 cm for Lake Vänern, 0.5 cm for Lake Okeechobee, and 0.6 cm for the Amazon River). Although the biases between the physical and empirical retrackers were minimized using a neural network there still appears to be some excess noise in these datasets compared to those that are obtained purely from empirical retrackers.

4.4. Time series

The time series obtained for the three study areas are shown in Fig. 8(a)–(c). The available in situ water levels have been included for comparison and the corresponding RMSEs are given in Table 6.

The time series for Lake Vänern in Fig. 8(a) shows a complicated pattern, which is captured well with satellite altimetry. The water level time series Lake Vänern cannot be resolved by a simple sine or cosine function, and varies less than a metre for the entire time period. The lowest RMSEs are obtained with the SAMOSA3-O retracker, but it should be noted that the SAMOSA3-O dataset only include results from the well-behaved waveforms. Comparing the RMSEs obtained from the NPPR and MWaPP methods for only these observations reveal similar performances.

When using all observations to derive time series data the RMSEs are slightly higher. The results from the MWaPP retracker give an RMSE around 5 cm, whereas the NPPR method has an RMSE around 11 cm. The RMSE values show that combining the physical and empirical retrackers do not offer more accurate time series data.

The time series over Okeechobee reveals that the mean values from MWaPP and the combined method with MWaPP values are almost identical. In fact, the mean absolute difference is only half a centimetre. Looking at the RMSE values we see the same thing

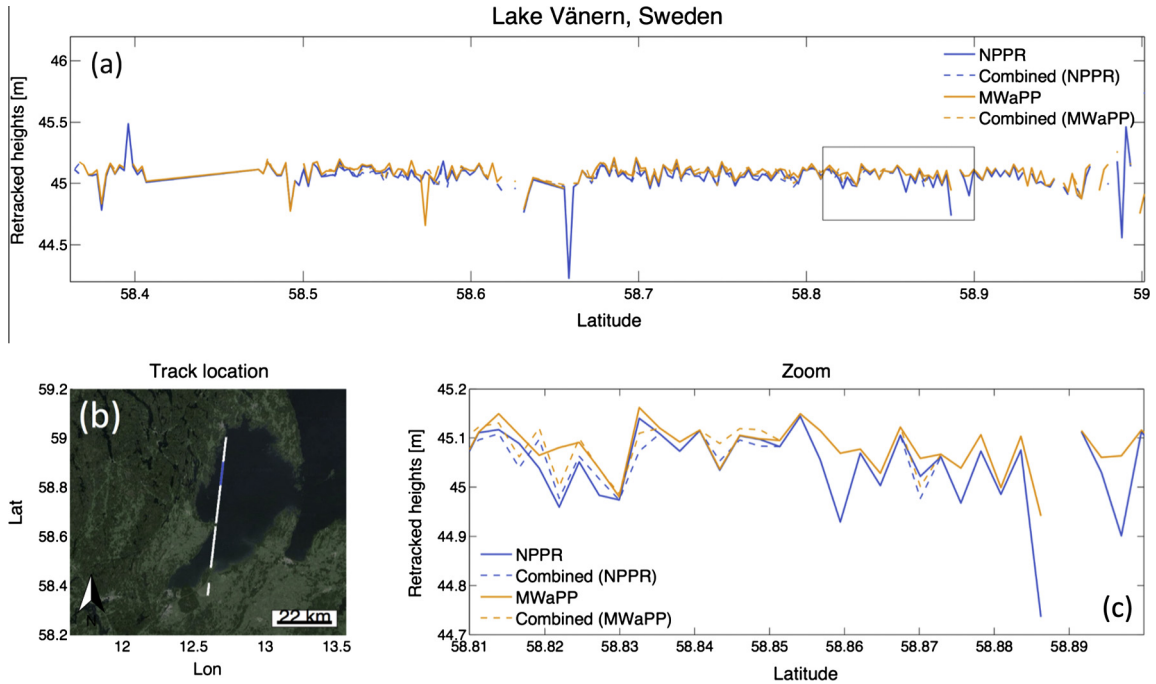


Fig. 6. (a) Comparison of retracking methods over Lake Vänern for a track on October 31st, 2011. (b) Track location across the lake. Highlighted (blue) points mark the observations shown in the detailed plot of (a) in (c). (For interpretation of the references to colour in this figure legend, the reader is referred to the web version of this article.)

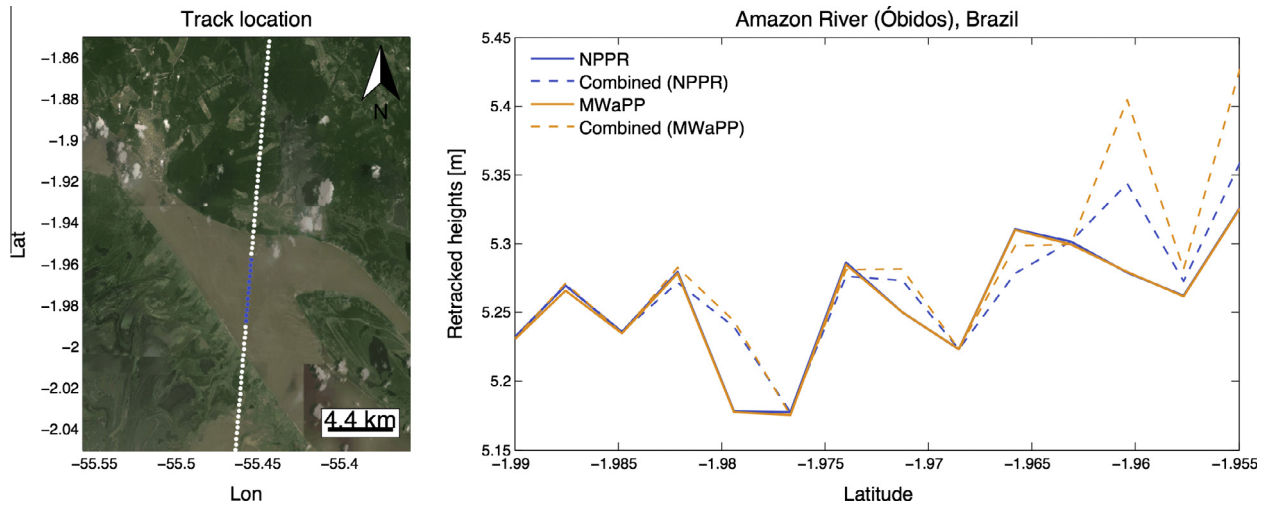


Fig. 7. Comparison of retracking methods over the Amazon River for a track crossing the river on October 2nd, 2012.

Table 4

Mean track standard deviations for the different methods for all available observations. Mean number of available observations per track is written in square brackets. Best results are highlighted in bold font.

Retracking method	Lake Vänern	Lake Okeechobee	Amazon River (Óbidos)
NPPR	15.3 cm [109]	39.2 cm [98]	29.9 cm [16]
MWaPP	9.1 cm [110]	13.4 cm [98]	29.0 cm [16]
Combined (SAMOSA3 + NPPR)	15.9 cm [109]	40.1 cm [98]	30.0 cm [16]
Combined (SAMOSA3 + MWaPP)	9.8 cm [110]	13.9 cm [99]	29.5 cm [16]
ESA L2	53.9 cm [107]	78.8 cm [95]	82.6 cm [16]

as in Lake Vänern, i.e. that the MWaPP retracker provides heights that follow the in situ levels much closer than the NPPR method. Again, the SAMOSA3-O retracker agrees the best with in situ data (2.1 cm), but with the corresponding RMSEs for NPPR and MWaPP are almost as low (2.4 cm)

For the Amazon River, the MWaPP retracker performs slightly worse than the NPPR method with RMSEs around 38–39 cm and 33 cm, respectively. The RMSE is more than halved when including only well-behaved waveforms for which the SAMOSA3-O retracker works (~15 cm).

Table 5
Mean track standard deviations for the different methods for waveforms where both SAMOSA3 retracker have correlations higher than 99%. Mean number of available observations per track is written in square brackets. Best results are highlighted in bold font.

Retracking method	Lake Vänern	Lake Okeechobee	Amazon River (Óbidos)
NPPR	5.3 cm [28]	4.4 cm [34]	3.2 cm [3]
MWaPP	5.2 cm [28]	4.3 cm [34]	3.5 cm [3]
Combined (SAMOSA3 + NPPR)	4.7 cm [28]	4.4 cm [35]	2.8 cm [3]
Combined (SAMOSA3 + MWaPP)	4.7 cm [28]	4.3 cm [34]	3.3 cm [3]
SAMOSA3-O	4.2 cm [26]	3.9 cm [32]	3.4 cm [3]
ESA L2	9.6 cm [28]	9.9 cm [34]	4.8 cm [3]

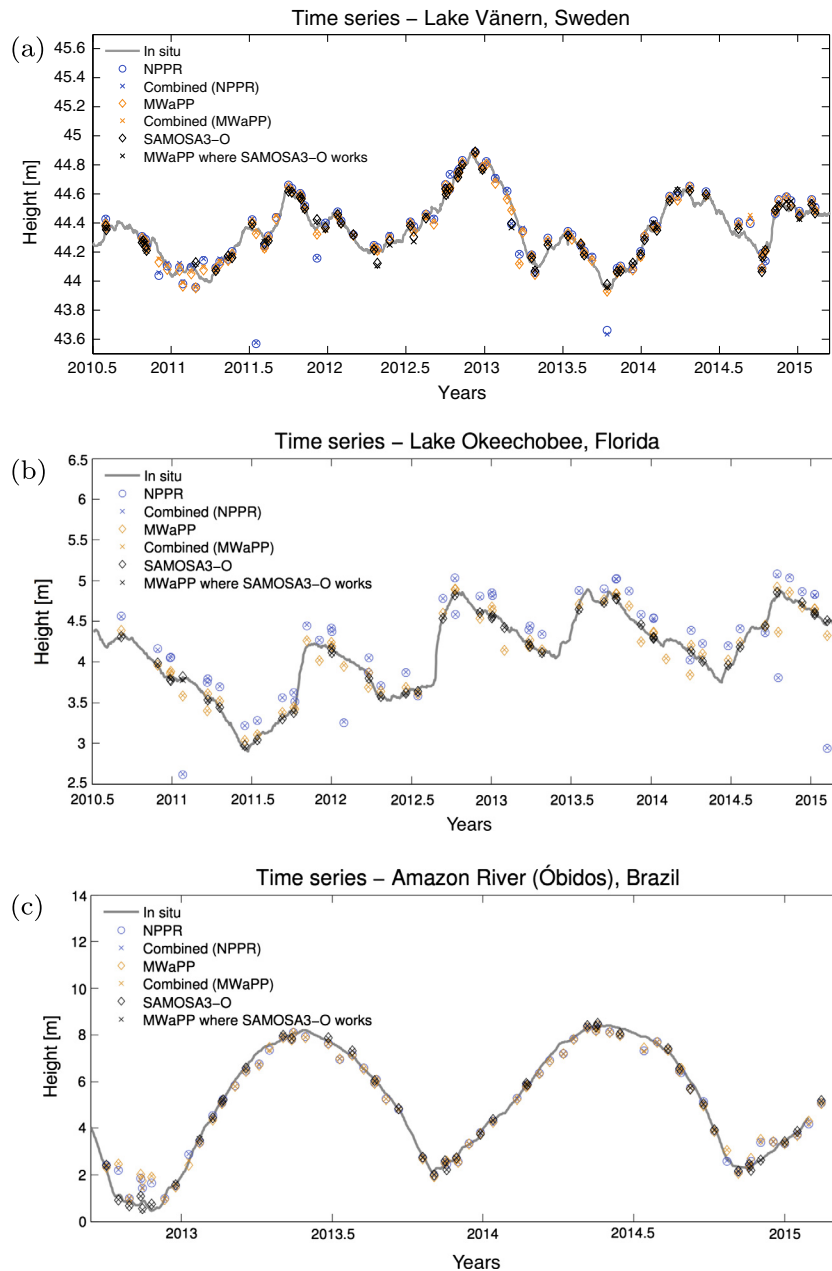


Fig. 8. Time series for the three different study areas derived from retracted heights and compared with in situ data.

5. Discussion

In general the studies presented here show great results from all retracker, but it is clear that the MWaPP retracker is able to retrieve heights from complex waveforms that would, if using other retracker, result in erroneous height estimates. The method

has a very low computational cost compared to the SAMOSA3 model, and although the results from the SAMOSA3-O retracker are better, i.e. have higher precisions and lower RMSEs, it is debatable whether or not the time consuming implementation/fitting and high number of discarded waveforms is worth the gain in precision.

Table 6

RMSEs between retracked heights and in situ water levels for Lake Vänern and Lake Okeechobee. The numbers in the parentheses are the same statistics but only including the observations where the SAMOSA3-O retracker could be used. Total number of available mean water levels is written in square brackets.

Retracking method	Lake Vänern	Lake Okeechobee	Amazon River (Óbidos)
NPPR	10.9 cm [86] (5.1 cm [70])	61.8 cm [55] (2.4 cm [43])	33.3 cm [66] (14.7 cm [41])
MWaPP	5.0 cm [86] (3.8 cm [70])	12.6 cm [55] (2.4 cm [43])	38.5 cm [66] (15.0 cm [41])
Combined (SAMOSA3 + NPPR)	10.9 cm [86]	61.6 cm [55]	33.2 cm [66]
Combined (SAMOSA3 + MWaPP)	5.1 cm [86]	12.3 cm [55]	38.3 cm [66]
SAMOSA3-O	3.5 cm [70]	2.1 cm [43]	15.3 cm [41]
ESA L2	47.0 cm [86]	121.9 cm [55]	88.8 cm [66]

Compared to the studies summarized in Table 1 the results for Lake Vänern and Lake Okeechobee are very encouraging. The lowest RMSE of 2.1 cm obtained from the SAMOSA3-O retracker over Lake Okeechobee is especially impressive considering the geodetic orbit of the CryoSat-2 satellite and the size of Lake Okeechobee compared to the other study regions presented in Table 1. However, it should be noted that the results from the SAMOSA3-O retracker are only obtained for well-behaved waveforms. Therefore, the RMSEs from the MWaPP retracker of 4.9 cm and 12.6 cm for Lake Vänern and Okeechobee, respectively, are more comparable to the values listed in Table 1.

There is no doubt that the SAMOSA3 retracker provides very stable water levels. The benefit of using the SAMOSA3 retracker is however concealed in regions like inland water where complicated waveforms are repeatedly encountered and an empirical retracker is needed as well. Trying to avoid the offset between the physical and empirical retrackers by adjusting the 80% threshold level for the empirical retrackers was unsuccessful. Therefore, in this study the offset is reduced using a neural network. From the results presented here, combining the physical and empirical retrackers does not seem to offer a higher level of precision or agreement with in situ data compared to using purely empirical retrackers. Indeed, the results presented here indicate that the bias issues that are introduced when combining retrackers mask the potential benefits of combining retrackers. Many of the outliers causing the higher RMSE of the NPPR dataset could of course have been avoided by using more sophisticated outlier detection methods, such as done in Nielsen et al. (2015b), but the MWaPP method presented in this study allows for retrieval of a higher number of useful heights, which is preferred in data sparse regions, such as narrow rivers or places with few useable height estimates.

There are many error sources for inland water altimetry, and it is hard to expect RMSEs lower than 2–3 cm. The geophysical corrections available over inland water are associated with several limitations (Fernandes et al., 2014), especially over smaller lakes and rivers. Comparing with in situ data also provides a source of error, as there might be a time lag between the time of the two water level measurements. In this study, daily gauge data were used, which could introduce some error depending on the rate at which the water level changes. The location of the gauge station also impacts the results, e.g. in case of strong winds, where water might be retained in certain areas of the lake, or if the river morphology differs from place to place, causing higher water levels in some areas, and lower in others. The orbit determination error is assumed to be less than 1 cm as according to Jayles et al. (2015). With all these potential error sources in mind, the results obtained in this and previous studies are not expected to improve further for lakes, but with sophisticated retracking and data editing, lower RMSEs might be obtainable for rivers. For Lake Vänern, freezing in winter might cause erroneous height estimates, which was not taken into account in this study. Apart from relatively large discrepancies between retracked and in situ data during the winter 2010/2011, which could be due to ice-cover during a cold winter, freezing of the lake does not seem to affect the presented results. After looking at historical temperature data from Karlstad just north of Lake

Vnern, it was witnessed that the air temperature often drops below zero in the period December–March, during which period parts of the lake might be covered with ice. When data from these months are removed from the analysis, we obtain slightly lower RMSEs for the MWaPP and SAMOSA-O retrackers of 4.0 cm and 3.3 cm, respectively. For the NPPR method, removing the winter data resulted in an RMSE of 12.4, i.e. a slight increase.

6. Conclusions and outlook

In this study we presented a number of novel methods for retracking CryoSat-2 SAR waveforms over inland water, especially the new way of taking adjacent waveforms into account during retracking to find the subwaveform that is most likely to hold the echo from the water body at nadir. We also presented a combined method that uses an empirical retracker as well as the SAMOSA3 model with retracking offsets minimized using a neural network approach.

The results showed that the SAMOSA3 model outperformed the other retrackers. However, the results were not much better than those obtained using the empirical MWaPP retracker presented in this study. When combining the physical and empirical retrackers, the higher precision of the SAMOSA3 model is concealed by the retracking offsets even after these were minimized using a neural network. Due to these findings we suggest using the proposed MWaPP developed for this study in regions where most waveforms cannot be retracked by the SAMOSA3 model. In bigger lakes with a high number of observations it could prove more beneficial to use the SAMOSA3 retrackers, especially if information on significant wave height or roughness is desirable, and simply discard waveforms where an acceptable fit is not obtainable.

To further improve precisions and RMSEs, we also suggest using more sophisticated methods for outlier detection and determination of robust mean water levels such as described in Nielsen et al. (2015b). Finally, it should be noted that the methods derived here are used on CryoSat-2 data, but should be easily applicable to any SAR data (such as from the upcoming Sentinel-3 mission) with only a few simple adjustments of the many parameters in the SAMOSA3 model. Sentinel-3 and its SRAL SAR altimeter will improve the possibilities for inland water monitoring even further with the repeat orbit of 27 days.

Acknowledgements

We would like to thank the European Space Agency (ESA) for providing CryoSat-2 data. This research was conducted with support from the EU FP7 LOTUS project (Preparing Land and Ocean Take Up From Sentinel-3) – Grant No. 313238. A special thank you to the SAMOSA team and Dr. Maulik Jain for providing the MATLAB codes necessary for the implementation of their model. We would also like to thank the three reviewers for their suggestions and comments, which greatly improved this manuscript. All map data were provided by Google Earth (SIO, NOAA, U.S. Navy, NGA, GEBCO and Landsat).

References

- Armitage, T.W.K., Davidson, M.W.J., 2014. Using the interferometric capabilities of the ESA CryoSat-2 mission to improve the accuracy of sea ice freeboard retrievals. *IEEE Trans. Geosci. Remote Sens.* 52, 529–536. <http://dx.doi.org/10.1109/TGRS.2013.2242082>.
- Bao, L., Lu, Y., Wang, Y., 2009. Improved retracking algorithm for oceanic altimeter waveforms. *Prog. Nat. Sci.* 19, 195–203. <http://dx.doi.org/10.1016/j.pnsc.2008.06.017>.
- Beale, M.H., Hagan, M.T., Demuth, H.B., 2015. *Neural Network Toolbox: Users Guide*. Matlab – MathWorks (accessed 06.02.15).
- Beaver, J.R., Casamatta, D.A., East, T.L., Havens, K.E., Rodusky, A.J., James, R.T., Tausz, C.E., Buccier, K.M., 2013. Extreme weather events influence the phytoplankton community structure in a large lowland subtropical lake (Lake Okeechobee, Florida, USA). *Hydrobiol. Int. J. Limnol. Mar. Sci.* 709, 213–226. <http://dx.doi.org/10.1007/s10750-013-1451-7>.
- Berry, P., 2006. Two decades of inland water monitoring using satellite radar altimetry. *Proceedings of the Symposium on 15 Years of Progress in Radar Altimetry*, 614. ESA Special Publication, p. 8.
- Berry, P.A.M., Garlick, J.D., Freeman, J.A., Mathers, E.L., 2005. Global inland water monitoring from multi-mission altimetry. *Geophys. Res. Lett.*, 32 <http://dx.doi.org/10.1029/2005GL022814>.
- Biancamaria, S., Hossain, F., Lettenmaier, D.P., 2011. Forecasting transboundary river water elevations from space. *Geophys. Res. Lett.* 38. <http://dx.doi.org/10.1029/2011GL047290>, n/a–n/a.
- Birkett, C., 1995. The contribution of TOPEX/POSEIDON to the global monitoring of climatically sensitive lakes. *J. Geophys. Res. – Oceans* 100, 25179–25204.
- Birkett, C., Reynolds, C., Beckley, B., Doorn, B., 2011. From research to operations: the USDA global reservoir and lake monitor. In: Vignudelli, S., Kostianoy, A.G., Cipollini, P., Benveniste, J. (Eds.), *Coastal Altimetry*. Springer, Berlin, Heidelberg, pp. 19–50. http://dx.doi.org/10.1007/978-3-642-12796-0_2.
- Birkett, C.M., 1994. Radar altimetry: a new concept in monitoring lake level changes. *Eos Trans. Am. Geophys. Union* 75, 273. <http://dx.doi.org/10.1029/94eo00944>.
- Birkett, C.M., 1998. Contribution of the TOPEX NASA radar altimeter to the global monitoring of large rivers and wetlands. *Water Resour. Res.* 34, 1223–1239. <http://dx.doi.org/10.1029/98WR00124>.
- Birkinshaw, S.J., O'Donnell, G.M., Moore, P., Kilsby, C.G., Fowler, H.J., Berry, P.A.M., 2010. Using satellite altimetry data to augment flow estimation techniques on the Mekong River. *Hydrol. Process.* 24, 3811–3825. <http://dx.doi.org/10.1002/hyp.7811>.
- Brakenridge, G.R., Cohen, S., Kettner, A.J., De Groeve, T., Nghiem, S.V., Syvitski, J.P.M., Fekete, B.M., 2012. Calibration of satellite measurements of river discharge using a global hydrology model. *J. Hydrol.* 475, 123–136. <http://dx.doi.org/10.1016/j.jhydrol.2012.09.035>.
- Cochonneau, G., Sondag, F., Martinez, J.-M., Seyler, F., Sidgwick, J., Guyot, J.-L., Fraizy, P., Geraldo, B., Filizola, M., Laraque, A., Magat, P., Noriega, L., Oliveira, E., Ordonez, J., Pombosa, R., Vauchel, P., 2006. The Environmental Observation and Research Project. ORE HYBAM, and the Rivers of the Amazon Basin.
- Cretaux, J.-F., Birkett, C., 2006. Lake studies from satellite radar altimetry. *C.R. Geosci.* 338, 1098–1112. <http://dx.doi.org/10.1016/j.crte.2006.08.002>.
- Crétaux, J.-F., Jelinski, W., Calmant, S., Kouraev, A., Vuljinski, V., Bergé-Nguyen, M., Gennero, M.-C., Nino, F., Rio, R.A.D., Cazenave, A., Maisongrande, P., 2011. SOLS: a lake database to monitor in the Near Real Time water level and storage variations from remote sensing data. *Adv. Space Res.* 47, 1497–1507. <http://dx.doi.org/10.1016/j.asr.2011.01.004>, <<http://www.sciencedirect.com/science/article/pii/S0273117711000287>>.
- Dave, G., Munawar, M., Wngberg, S., 2015. Ecosystem health of Lake Vänern: past, present and future research. *Aquat. Ecosyst. Health Manage.* 18, 205–211. <http://dx.doi.org/10.1080/14634988.2015.1017437>.
- Dinardo, S., Lucas, B., Gommenginger, C., Martin-Puig, C., et al., 2013. Detailed Processing Model of the Sentinel-3 SRAL SAR Altimeter Sea Waveform Retracker v2.3.0.
- Dyer, J., Garza, R., 2004. A comparison of precipitation estimation techniques over Lake Okeechobee, Florida. *Weather Forecast.* 19, 1029–1043.
- ESA and Mullard Space Science Laboratory – University College London, 2012. *CryoSat Product Handbook*.
- Fernandes, M.J., Lazaro, C., Nunes, A.L., Scharroo, R., 2014. Atmospheric corrections for altimetry studies over inland water. *Remote Sens.* 6, 4952–4997.
- Fetterer, F.M., Drinkwater, M.R., Jezek, K.C., Laxon, S.W.C., Onstott, R.G., Ulander, L. M.H., 2013. Sea ice altimetry. In: *Microwave Remote Sensing of Sea Ice*. American Geophysical Union, pp. 111–135. <http://dx.doi.org/10.1029/GM068p0111>.
- Gomez-Enri, J., Vignudelli, S., Quartly, G.D., Gommenginger, C.P., Cipollini, P., Challenor, P.G., Benveniste, J., 2010. Modeling ENVISAT RA-2 waveforms in the coastal zone: case study of calm water contamination. *IEEE Geosci. Remote Sens. Lett.* 7, 474–478. <http://dx.doi.org/10.1109/LGRS.2009.2039193>.
- Gommenginger, C., Thibaut, P., Fenoglio-Marc, L., Quartly, G., Deng, X., Gomez-Enri, J., Challenor, P., Gao, Y., 2011. Retracking altimeter waveforms near the coasts: a review of retracking methods and some applications to coastal waveforms. *Coast. Altimetry*, 61–101. http://dx.doi.org/10.1007/978-3-642-12796-0_4.
- Idris, N.H., 2014. Development of New Retracking Methods for Mapping Sea Levels over the Shelf Areas from Satellite Altimetry Data. Ph.D. Thesis. The University of Newcastle Australia.
- Jain, M., 2015. Improved Sea Level Determination in the Arctic Regions Through Development of Tolerant Altimetry Retracking. Ph.D. Thesis DTU Space. Technical University of Denmark.
- Jain, M., Andersen, O.B., Dall, J., Stenseng, L., 2015. Sea surface height determination in the Arctic using CryoSat-2 (SAR) data from primary peak empirical retrackers. *Adv. Space Res.* 55, 40–50. <http://dx.doi.org/10.1016/j.asr.2014.09.006>, <<http://www.sciencedirect.com/science/article/pii/S0273117714005705>>.
- Jain, M., Martin-Puig, C., Andersen, O.B., Stenseng, L., Dall, J., 2014. Evaluation of SAMOSA3 adapted retracker using CryoSat-2 SAR altimetry data over the Arctic ocean, pp. 5115–5118. <http://dx.doi.org/10.1109/IGARSS.2014.6947648>.
- Jarihani, A.A., Callow, J.N., Johansen, K., Gouweleeuw, B., 2013. Evaluation of multiple satellite altimetry data for studying inland water bodies and river floods. *J. Hydrol.* 505, 78–90. <http://dx.doi.org/10.1016/j.jhydrol.2013.09.010>.
- Jayles, C., Chauveau, J.-P., Auriol, A., 2015. DORIS/DIODE: real-time orbit determination performance on board SARAL/AltiKa. *Mar. Geodesy* 38, 233–248. <http://dx.doi.org/10.1080/01490419.2015.1015695>.
- Kleinherenbrink, M., Ditmar, P., Lindenberg, R., 2014. Retracking CryoSat data in the SARIn mode and robust lake level extraction. *Remote Sens. Environ.* 152, 38.
- Kleinherenbrink, M., Lindenberg, R., Ditmar, P., 2015. Monitoring of lake level changes on the Tibetan Plateau and Tian Shan by retracking CryoSat (SARIn) waveforms. *J. Hydrol.* 521, 119–131. <http://dx.doi.org/10.1016/j.jhydrol.2014.11.063>, <<http://www.sciencedirect.com/science/article/pii/S0022169414009858>>.
- Koblinsky, G.J., Clarke, R.T., Brenner, A.C., Frey, H., 1993. Measurement of river level variations with satellite altimetry. *Water Resour. Res.* 29, 1839–1848. <http://dx.doi.org/10.1029/93WR00542>.
- Lehner, B., Doll, P., 2004. Development and validation of a global database of lakes, reservoirs and wetlands. *J. Hydrol.* 296, 1–22. <http://dx.doi.org/10.1016/j.jhydrol.2004.03.028>.
- Maillard, P., Bercher, N., Calmant, S., 2015. New processing approaches on the retrieval of water levels in Envisat and SARAL radar altimetry over rivers: a case study of the Sao Francisco River, Brazil. *Remote Sens. Environ.* 156, 226–241. <http://dx.doi.org/10.1016/j.rse.2014.09.027>.
- Michailovsky, C.I., McEnnis, S., Berry, P.A.M., Smith, R., Bauer-Gottwein, P., 2012. River monitoring from satellite radar altimetry in the Zambezi River Basin. *Hydrol. Earth Syst. Sci. Discuss.* 9, 3203–3235. <http://dx.doi.org/10.5194/hessd-9-3203-2012>.
- Michailovsky, C.I., Milzow, C., Bauer-Gottwein, P., 2013. Assimilation of radar altimetry to a routing model of the Brahmaputra River. *Water Resour. Res.* 49, 4807–4816. <http://dx.doi.org/10.1002/wrcr.20345>.
- Neal, J., Schumann, G., Bates, P., Buytaert, W., Matgen, P., Pappenberger, F., 2009. A data assimilation approach to discharge estimation from space. *Hydrol. Process.* 23, 3641–3649. <http://dx.doi.org/10.1002/hyp.7518>.
- Nielsen, K., Stenseng, L., Andersen, O., Villadsen, H., Knudsen, P., 2015. Validation of lake levels based on CryoSat-2 SAR mode data. In: Presented at the Sentinel-3 for Science Workshop, Venice, Italy (June 2015).
- Nielsen, K., Stenseng, L., Andersen, O.B., Villadsen, H., Knudsen, P., 2015b. Validation of CryoSat-2 SAR mode based lake levels. *Remote Sens. Environ.* 171, 162–170. <http://dx.doi.org/10.1016/j.rse.2015.10.023>.
- Pavlis, N.K., Holmes, S.A., Kenyon, S.C., Factor, J.K., 2012. The development and evaluation of the earth gravitational model 2008 (EGM2008). *J. Geophys. Res. – Solid Earth*, 117. <http://dx.doi.org/10.1029/2011JB008916>.
- Quartly, G., 2010. Hyperbolic retracker: removing bright target artefacts from altimetric waveform data. In: *ESA Living Planet Symposium*, Bergen, 28th Jun–2nd July 2010.
- Raney, R.K., 1998. The delay/Doppler radar altimeter. *IEEE Trans. Geosci. Remote Sens.* 36, 1578–1588. <http://dx.doi.org/10.1109/36.718861>.
- Ray, C., Martin-Puig, C., Clarizia, M.P., Ruffini, G., Dinardo, S., Gommenginger, C., Benveniste, J., 2015. SAR altimeter backscattered waveform model. *IEEE Trans. Geosci. Remote Sens.* 53, 911–919. <http://dx.doi.org/10.1109/TGRS.2014.2330423>.
- Rudorff, C.M., Melack, J.M., Bates, P.D., 2014. Flooding dynamics on the lower Amazon floodplain: 2. Seasonal and interannual hydrological variability. *Water Resour. Res.* 50, 635–649. <http://dx.doi.org/10.1002/2013WR014714>.
- Schwatke, C., Dettmering, D., Boergens, E., Bosch, W., 2015a. Potential of SARAL/AltiKa for inland water applications. *Mar. Geodesy* 38, 626–643. <http://dx.doi.org/10.1080/01490419.2015.1008710>.
- Schwatke, C., Dettmering, D., Bosch, W., Seitz, F., 2015b. Kalman filter approach for estimating water level time series over inland water using multi-mission satellite altimetry. *Hydrol. Earth Syst. Sci. Discuss.* 12, 4813–4855. <http://dx.doi.org/10.5194/hessd-12-4813-2015>, <<http://www.hydrol-earth-syst-sci-discuss.net/12/4813/2015/>>.
- Seppl, M., 2005. *The Physical Geography of Fennoscandia*. The Oxford Regional Environments Series. Oxford University Press, <<http://ci.nii.ac.jp/ncid/BA80490866>>.
- da Silva, J.S., Calmant, S., Seyler, F., Rotunno Filho, O.C., Cochonneau, G., Mansur, W. J., 2010. Water levels in the Amazon basin derived from the ERS 2 and ENVISAT radar altimetry missions. *Remote Sens. Environ.* 114, 2160–2181. <http://dx.doi.org/10.1016/j.rse.2010.04.020>.
- Song, C., Huang, B., Ke, L., 2014. Inter-annual changes of alpine inland lake water storage on the Tibetan Plateau: detection and analysis by integrating satellite altimetry and optical imagery. *Hydrol. Process.* 28, 2411–2418. <http://dx.doi.org/10.1002/hyp.9798>.

- Thibaut, J., Aublanc, P., Moreau, T., Boy, F., Picot, N., 2014. Delay/Doppler waveform processing in coastal zones. In: 8th Coastal Altimetry Workshop – Konstanz, Germany.
- Tourian, M., Elmi, O., Chen, Q., Devaraju, B., Roohi, S., Sneeuw, N., 2015. A spaceborne multisensor approach to monitor the desiccation of Lake Urmia in Iran. *Remote Sens. Environ.* 156, 349–360. <http://dx.doi.org/10.1016/j.rse.2014.10.006>, <<http://www.sciencedirect.com/science/article/pii/S0034425714004027>>.
- Vignudelli, S., Kostianoy, A., Cipollini, P., Benveniste, J., 2010. *Coastal Altimetry*. Springer, Berlin, Heidelberg, <https://books.google.com/books?id=M_2ljwEACAAJ>.
- Villadsen, H., Andersen, O., Stenseng, L., Nielsen, K., Knudsen, P., 2015. CryoSat-2 altimetry for river level monitoring – evaluation in the Ganges-Brahmaputra River basin. *Remote Sens. Environ.* 168, 80–89. <http://dx.doi.org/10.1016/j.rse.2015.05.025>.
- Wingham, D., Francis, C., Baker, S., Bouzinac, C., Brockley, D., Cullen, R., de Chateau-Thierry, P., Laxon, S., Mallow, U., Mavrocordatos, C., Phalippou, L., Ratier, G., Rey, L., Rostan, F., Viau, P., Wallis, D., 2006. CryoSat: a mission to determine the fluctuations in Earth's land and marine ice fields. *Adv. Space Res.* 37, 841–871. <http://dx.doi.org/10.1016/j.asr.2005.07.027>.
- Yi, Y., Kouraev, A.V., Shum, C.K., Vuglinsky, V.S., Cretaux, J.-F., Calmant, S., 2013. The performance of altimeter waveform retracers at Lake Baikal. *Terr. Atmos. Ocean. Sci.* 24, 513–519. [http://dx.doi.org/10.3319/tao.2012.10.09.01\(tibxs\)](http://dx.doi.org/10.3319/tao.2012.10.09.01(tibxs)).
- Zakharova, E.A., Kouraev, A.V., Rmy, F., Zemtsov, V.A., Kirpotin, S.N., 2014. Seasonal variability of the Western Siberia wetlands from satellite radar altimetry. *J. Hydrol.* 512, 366–378. <http://dx.doi.org/10.1016/j.jhydrol.2014.03.002>.